Journal of Hydrology 578 (2019) 124097

Contents lists available at ScienceDirect

Journal of Hydrology

journal homepage: www.elsevier.com/locate/jhydrol

Research papers

Experimental investigation of thermal retardation and local thermal non-equilibrium effects on heat transport in highly permeable, porous aquifers

Manuel A. Gossler[a], Peter Bayer[b], Kai Zosseder[a,*]

[a] Technical University of Munich, Arcisstraße 21, 80333 Munich, Germany
[b] Ingolstadt University of Applied Sciences, Esplanade 10, 85049 Ingolstadt, Germany

ARTICLE INFO

This manuscript was handled by Huaming Guo, Editor-in-Chief, with the assistance of Xu-Sheng Wang, Associate Editor

Keywords:
Local thermal equilibrium
Local thermal non-equilibrium
Heat tracer
Solute tracer
Laboratory experiment
Thermal retardation

ABSTRACT

Actively stimulated temperature changes are common in many groundwater applications. A widely used concept to determine water fluxes, mean transit times, and other parameters from heat tracer tests is the use of the thermal retardation factor. Different methods are available to determine the thermal velocity from thermal breakthrough curves (BTCs) depending on the input signal. This study systematically compares these methods and investigates possible local thermal non-equilibrium effects (LTNE) in coupled solute and heat tracer experiments for highly permeable, porous aquifers. One-dimensional column experiments with saturated gravel of grain size 7–15 mm are conducted to compare the measured, effective thermal retardation with the computed thermal retardation predicted by the apparent thermal retardation factor. The results demonstrate that for scenarios with a step input of the heat tracer, the effective thermal retardation for thermal velocities derived by an analytical model, and the mean between injection temperature and initial temperature, can be predicted by the apparent thermal retardation factor. This indicates that possible LTNE effects do not significantly influence the derived velocities within the investigated range of seepage velocity between 5 and 50 m d^{-1}. Other methods showed constant deviation from the apparent retardation factor at higher seepage velocities. In scenarios with a finite duration pulse input of the heat tracer, the effective retardation derived by the peak velocity showed deviations from the apparent retardation up to 35% at seepage velocities lower than 10 m d^{-1}. At higher seepage velocities, the peak velocity could be predicted by the apparent retardation factor.

1. Introduction

Knowledge of heat transport in aquifers is of primary interest in many areas of hydrogeological research and practice. For instance, shallow geothermal energy systems often use groundwater to exchange heat with the subsurface for heating, cooling or storage. Induced changes in the groundwater temperature depend on the relative dominance of heat conduction or advection, and in aquifers with high flow velocities especially, advective heat transport generates far-reaching thermal plumes (Banks, 2015; Seibertz et al., 2016; Maya et al., 2018). While robust estimation of the governing hydraulic and thermal parameters is crucial for system performance prediction (Hermans et al., 2018), it is also relevant for management of multiple adjacent installations. Thermal interference can mitigate technological performance, and it can yield temperature changes in the shallow groundwater beyond environmentally critical thresholds (Epting et al., 2017; Böttcher et al., 2019). Aside from the rising interest in groundwater effects of geothermal applications, the thermal conditions in aquifers are also studied in other contexts. Heat is considered a worthwhile tracer to characterize hydraulic properties and surface water-groundwater interactions, particularly in dynamic, highly permeable systems. (Anderson, 2005; Constantz, 2010; Saar, 2010; Rau et al., 2014; Halloran et al., 2016a; Klepikova et al., 2016a; Irvine et al., 2016, 2017; Kurylyk et al., 2018; Ren et al., 2018).

For interpreting heat as a tracer to describe groundwater flow in porous aquifers, commonly a local thermal equilibrium (LTE) is assumed (e.g. Hoehn and Cirpka, 2006; Markle and Schincariol, 2007; Stauffer et al., 2013; Bekele et al., 2014; Irvine et al., 2015; Sarris et al., 2018). This means that heat diffusion into the matrix is sufficiently quick at the thermal front so that any kinetic effects from delayed intra-particle diffusion can be ignored. As a consequence of heat diffusion, the thermal velocity is lower than the fluid velocity, quantified by the effective retardation factor, R_{eff}. If LTE is valid, R_{eff} equals an apparent retardation factor R_{app}, that is estimated by relating the ratio of heat capacities between bulk media and fluid.

However, increase of fluid flow velocity and particle size may cause

* Corresponding author at: Technical University of Munich, Chair of Hydrogeology, Arcisstraße 21, 80333 Munich, Germany.
E-mail address: kai.zosseder@tum.de (K. Zosseder).

https://doi.org/10.1016/j.jhydrol.2019.124097
Received 27 May 2019; Received in revised form 6 August 2019; Accepted 2 September 2019
Available online 04 September 2019

Nomenclature

A	cross-sectional area of the column [m^2]
c	specific heat capacity [J kg^{-1} K^{-1}]
D_l	longitudinal effective thermal dispersion [m^2 s^{-1}]
$distance_{Pt100}$	distance of temperature sensor from inflow [m]
e	thermal effusivity [J K^{-1} m^{-2} $s^{-0.5}$]
L	characteristic length [m]
M	mass of tracer [g]
n_{eff}	effective porosity [–]
n_{tot}	total porosity [–]
$\mathrm{Pe} = \frac{\rho_f c_f q L}{\lambda_b}$	thermal Péclet number [–]
P_D	dispersion parameter [–]
q	specific discharge [m s^{-1}]
Q	volume flow [m^3 s^{-1}]
R_{app}	apparent thermal retardation [–]
R_{eff}	effective thermal retardation [–]
r	radius of the column [m]
t	time [s]
t_{char}	characteristic time [s]

Subscripts:

s	solid
f	fluid
b	bulk saturated porous media
t_0	mean transit time [s]
T	bulk temperature of REV [°C]
T_0	initial temperature [°C]
T_{end}	injection temperature after the pulse [°C]
T_{inj}	injection temperature [°C]
v_a	seepage velocity [m d^{-1}]
$v_{thermfit}$	thermal velocity [m d^{-1}]
$v_{thermpeak}$	thermal peak velocity [m d^{-1}]
$v_{thermpeakdt/dT}$	thermal velocity of peak of first time derivative [m d^{-1}]
$v_{thermT25\|T50\|T75}$	thermal velocity corresponding to 0.25|0.50|0.75 of normalized thermal BTC [m d^{-1}]
x	distance [m]
$\alpha_l^t \left\lvert \frac{\rho_f c_f}{\rho_b c_b} q \right\rvert$	longitudinal thermal mechanical dispersion [m^2 s^{-1}]
α_l^s	longitudinal solute dispersivity [m]
α_l^t	longitudinal thermal dispersivity [m]
λ	thermal conductivity [W m^{-1} K^{-1}]
κ	thermal diffusivity [m^2 s^{-1}]
ρ	specific density [kg m^{-3}]
τ	pulse duration of injection [s]

local thermal non-equilibrium (LTNE) conditions (Zhang et al., 2009). This yields a difference in the theoretical $R_{app}$and the measured R_{eff}. When LTE is assumed for heat transport, the temperature difference between the solid and the fluid phase within a representative elementary volume (REV) is considered negligible. As summarized by Rau et al. (2014), this assumption may be violated under high flow conditions in material with a high non-uniformity. With high non-uniformity, the REV has to be correspondently bigger (Rau et al., 2014). Theoretical analysis showed that LTNE effects might occur in sediments. Roshan et al. (2014) argued that this will be limited to very low flow velocities. They reasoned that increasing flow velocities lead to higher advective fluxes, which increase the LTNE between the fluid and solid phase, but that this effect is significantly smaller than the increase of the heat transfer coefficient which comes along with increasing flow velocities leading to LTE conditions. In a laboratory experiment, Levec and Carbonell (1985) demonstrated that LTNE effects result in a separated thermal front with the solid phase lagging behind the fluid phase. This separation amplifies with increasing flow velocities (Levec and Carbonell, 1985). The higher thermal velocities in the fluid would lead to a lower effective thermal retardation. Whether this is likely to happen for Darcian flows in natural sediments has yet to be established and needs further investigation (Rau et al., 2014; Visser et al., 2015).

Experimental investigation of thermal retardation, and hence influences of LTNE, could be accomplished by comparison of a heat and a conservative solute tracer. However, this is complicated by the fundamental difference of heat transport through the solid and fluid phase, and of solute transport that is limited to the fluid phase. Solute diffusion and heat conduction usually differ in two to three orders of magnitude (Anderson, 2005). This can generate dissimilar thermal and solute transport regimes for the same Darcy flux, as these differences result in different Péclet numbers (Rau et al., 2012a). Moreover, the role of thermal mechanical dispersion for heat transport in porous media is not fully clear (Bear, 1972; Hopmans et al., 2002; Constantz et al., 2003; Irvine et al., 2013; Park et al., 2015, 2018). Specifically, this is the case regarding its relationship to the fluid velocity (linear or power law) and with respect to scale dependency (Metzger et al., 2004; Anderson, 2005; Vandenbohede et al., 2009; Rau et al., 2012a; Afshari et al., 2019). Bandai et al. (2017) concluded in a laboratory experiment that while solute dispersion is independent of particle size, thermal dispersion is influenced by it, most likely due to the LTNE effects of thermal transport.

Neglecting effective thermal dispersion would result in a breakthrough curve (BTC) with a sharp temperature front, which can easily be used to determine the thermal velocity, v_{therm} (Bodvarsson, 1972; Woods and Fitzgerald, 1993, 1997; Shook, 2001). However, in previous experimental studies listed in Table 1, measured thermal BTCs are influenced by conduction and thermal mechanical dispersion, resulting in a differently shaped BTC, depending on the used temperature signal. So these differences should be accounted for, when thermal BTCs from heat tracer tests are evaluated.

Studies which systematically investigate the flow velocities derived from heat tracers and solute tracers are scarce. (Taniguchi and Sharma, 1990; Rau et al., 2012a,b; Irvine et al., 2013; Bandai et al., 2017). Their results are also not consistent: some works reveal a good agreement (Irvine et al., 2013), while others found systematic over- or underestimation (Rau et al., 2012a,b; Bandai et al., 2017). Other studies used both heat and solute tracers, but did not make a systematic comparison between heat- and solute-derived velocities (Constantz et al., 2003; Vandenbohede et al., 2009; Ma et al., 2012; Seibert et al., 2014; Wildemeersch et al., 2014; Bakker et al., 2015; Becker et al., 2015; Klepikova et al., 2016b; Bonner et al., 2017; Sarris et al., 2018).

Collectively, it is revealed that heat transport and thermal BTCs in highly permeable, porous aquifers have not yet been thoroughly investigated. LTNE effects can impact heat transport, especially for high flow velocities, whereas methods to derive thermal velocities from BTCs are strongly influenced by conduction and thermal mechanical dispersion. The aim of this paper is to systematically evaluate such possible LTNE effects in highly permeable porous aquifers, and additionally, to examine crucial experimental settings for comparing heat and solute tracer propagation. In a series of laboratory tests with high seepage velocities between 5 and 50 m d^{-1}, we investigate the role of the applied thermal signal under different hydraulic conditions. Different methods are contrasted to determine the thermal velocity, and to correctly derive fluid velocities or the bulk heat capacity of the porous medium with the effective thermal retardation factor.

Table 1
Methods for different source signal types used to derive the thermal velocity, $v_{therm\ fit}$ as the velocity obtained by fitting an analytical model to a BTC, the peak velocity $v_{therm\ peak}$ and the peak velocity of the first time derivative $v_{therm\ peak\ dT/dt}$ from heat tracer experiments.

Source signal type	Methods to determine v_{therm}	Examples from literature
Finite duration pulse signal	Fitting parameter in analytical model ($v_{therm\ fit}$)	Bakker et al. (2015)
	Peak time ($v_{therm\ peak}$)	Taniguchi and Sharma (1990); Constantz et al. (2003); Lewandowski et al. (2011); Wagner et al. (2013); Somogyvári and Bayer (2017)
	Peak of first time derivative ($v_{therm\ peak\ dT/dt}$)	Somogyvári and Bayer (2017)
Step signal	Fitting parameter in analytical model ($v_{therm\ fit}$)	Rau et al. (2012a); Bandai et al. (2017)
	Self-defined value between initial and injection temperature	Park et al. (2015)
	Mean value between initial and injection temperature	Irvine et al. (2013)
	Peak of first time derivative ($v_{therm\ peak\ dT/dt}$)	Somogyvári et al. (2016)
Periodic signal	Fitting parameter in analytical model ($v_{therm\ fit}$)	Rau et al. (2012b, 2017); Halloran et al. (2016b); Schneidewind et al. (2016); Caissie and Luce (2017)
	Lag time from maximum cross correlation	Hoehn and Cirpka (2006); Markle and Schincariol (2007); Vandenbohede and Van Houtte (2012); Bekele et al. (2014); Taylor et al. (2016); Moeck et al. (2017)
	Characteristic peak and trough matching	Markle and Schincariol (2007); Laws et al. (2011); Becker et al. (2015)

2. Material and methods

Two series of experiments for a highly permeable, porous aquifer here consisting of gravel were conducted. For two different input signals, the seepage velocity was systematically varied between 5 and 50 m d^{-1} while other parameters of the were kept constant. The step input experiments were conducted with two different injection temperatures (see also Table 3).

2.1. Experimental method

2.1.1. Experimental setup

The laboratory setup illustrated in Fig. 1 was developed to study one-dimensional (1D) heat and solute tracer transport through a cylinder-shaped sample at seepage velocities of v_a = 1 – 50 m d^{-1} and at temperatures of 5–70 °C. To enable an instant change between hot water injection and cold water injection, two refrigerated bath circulators (Witeg WCR-P22) were used. The two devices have an accuracy of ± 0.1 K. They can be used independently for heating and cooling, and served here as cold and hot water tanks. An eight-channel peristaltic pump (Ismatec Ecoline) was used to control the volume flow into the column. A three-way valve was installed at each of the inflow tubes close to the column to allow tempering of the tubes without injection into the column. Furthermore, the three-way valves were used to inject a solute tracer.

The sample was inserted in an acrylic glass column with an inner diameter of 0.29 m and a length of 1.5 m. Uniform inflow and outflow of the column was ensured by eight radially arranged inlets (CPC

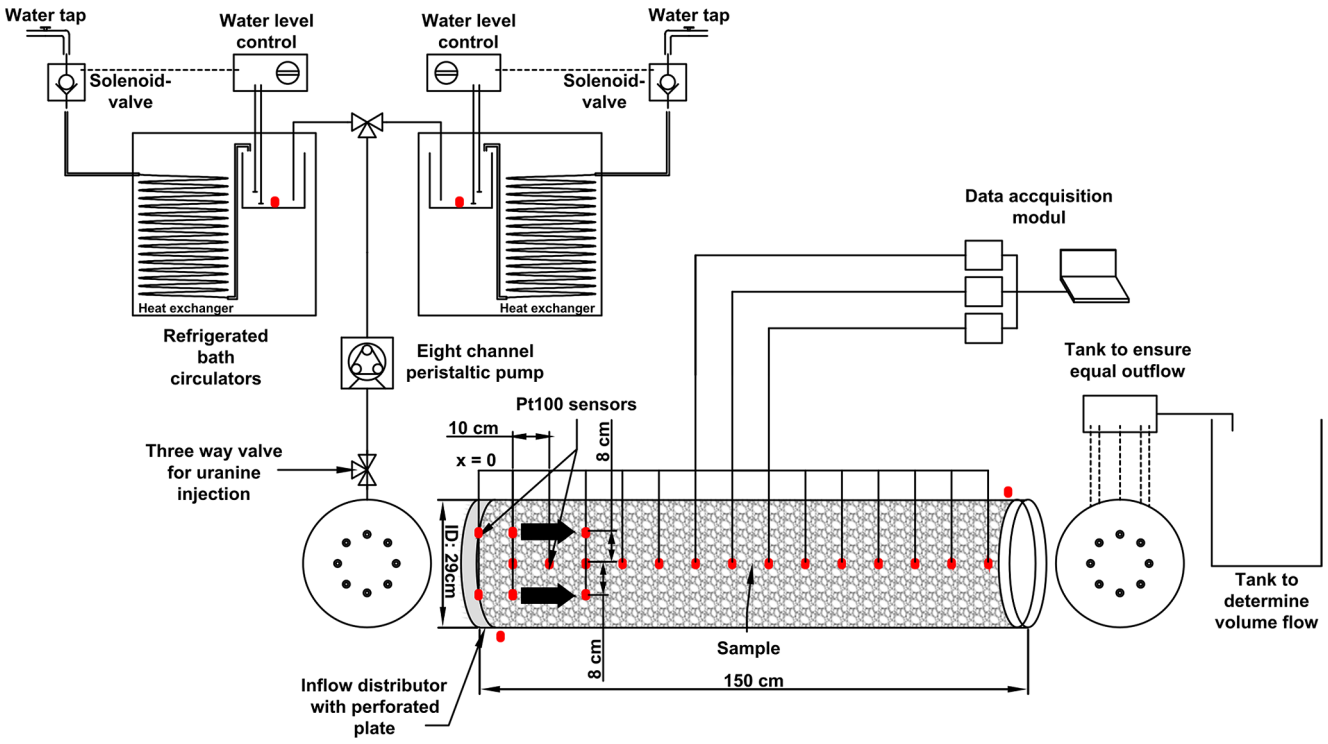

Fig. 1. Schematic experimental setup of the laboratory experiments. The refrigerated bath circulators served as a hot and cold water storage. The volume flow was controlled by an eight-channel peristaltic pump. The red dots mark the positions of the Pt100 temperature sensors. The column can be installed in a vertical and horizontal configuration. (For interpretation of the references to color in this figure legend, the reader is referred to the web version of this article.)

couplings) in the lid and the bottom of the column, and by an inflow distributor consisting of a perforated plate with a distance of 4 cm after the lid. The column was thermally insulated by a 5-cm-thick layer of K-Flex 25 ($\lambda = 0.034\ W\ m^{-1}\ K^{-1}$) insulation. In addition, the inflow tubes were thermally insulated by a K-Flex tube (wall thickness 10 mm). A tank at the end of the outflow tubes was installed to ensure the same pressure level at each outflow tube. In addition, a tank at the outflow was used to determine the volume flow through the column.

2.1.2. Data acquisition system for heat and solute

The temperature development of the fluid in the laboratory setup was monitored with four-wire Pt100 sensors (Omega Engineering) with an accuracy class 1/10 of IEC 751/EN 60,751 resulting in an accuracy of ± 0.03 K. Two kinds of Pt100 sensors were used: sheathed ones with a total length of 18 cm and a diameter of 3 mm, and hermetically sealed wire sensors with a diameter of 1 mm. During the packing of the column, these sensors were inserted from the outside of the column with thermo fittings. The sheathed sensors were positioned at the center of the column. Calibration was done using high precision bath circulators. In addition to the column itself, the temperature in the circulation thermostats and the room temperature were monitored. The positions of the sensors are shown in Fig. 1. The data acquisition at a 3 s interval was handled by Pt104A modules (Omega Engineering).

To determine seepage velocities and solute dispersivity, a solute tracer (uranine) was used. It was injected into the column with the fluid using the three-way valves. The samples were taken at the outflow of the column. The solute tracer was analyzed with a fluorescence spectrometer (Perkin Elmer LS 45). To each fluid sample, 20 µl of 20 wt% EDTA was added to reach a pH-value of approximately 9, and to avoid precipitation of interfering particles. A dilution series from a known concentration was measured to create a calibration curve using the measured intensities and the concentration. A linear regression of the calibration curve was used to calculate the concentration from the measured intensity. The measurement setup of the fluorescence spectrometer was: excitation wavelength of 491 nm and detection wavelength of 512 nm.

2.1.3. Properties of the porous media

The gravel used as the sample in the laboratory setup was sieved Carrara Marble, with a grain size distribution in the range of 7–15 mm. The following properties are needed to calculate the apparent thermal retardation for the porous medium: The total porosity n_{tot} of the saturated gravel was experimentally determined three times in a two-step procedure. First, the specific density of the marble was obtained by measuring the volume (water displacement) and the weight. In the second step, a circular vessel with a diameter of 26 cm and a height of 25 cm was filled with gravel and compacted with the same method as during column packing. The weight of the gravel (~8.5 kg) was measured. Then, water was added until the surface of the topmost gravel was covered and the total weight was determined. The specified parameter values were used to derive the volume of the gravel and the water and thereby, n_{tot}. The temperature during the experiments was 24.5 °C, the accuracy of the scale was ± 0.1 g. The resulting calculated total porosity was $n_{tot} = 36 \pm 1\%$. The effective porosity n_{eff} was determined with solute tracer tests, as described below in Chap. 3.1. The volumetric heat capacity $\rho_s c_s$ of the gravel was estimated by a modified transient plane source method with a commercial device (C-therm) by:

$$\rho_s c_s = \frac{e_s^2}{\lambda_s}, \tag{1}$$

whereas the solid thermal effusivity, e_s, and thermal conductivity λ_s of the saturated solid phase were measured (He, 2005). The used contact agent was distilled water and the measurement time was 1 s. Three pieces of gravel with a diameter of approximately 40 mm were cut in half, resulting in 6 samples. The surface was polished until smooth to assure optimal contact to the sensor. Before the measurement, the pieces of gravel were saturated in water for 24 h.

The bulk volumetric heat capacity of the saturated porous media $\rho_b c_b$ is defined as (Buntebarth and Schopper, 1998; Scharli and Rybach, 2001):

$$\rho_b c_b = n_{tot}\rho_f c_f + (1 - n_{tot})\rho_s c_s \tag{2}$$

The thermal conductivity of the saturated gravel λ_b can be estimated by the geometric mean model (Tarnawski et al., 2011):

$$\lambda_b = \lambda_f^{n_{tot}} \lambda_s^{1-n_{tot}} \tag{3}$$

A summary of the properties of the properties of the porous medium is given in Table 2.

Table 2
Parameter values of the porous medium, measured or taken from literature.

Parameter	Unit	Value	Procedure / Source
Particle size	[mm]	7–15	based on vendor information (purchased material)
Total porosity n_{tot}	[%]	36 ± 1	measured
Effective porosity n_{eff}	[%]	35 ± 2	measured (solute tracer tests Eq. (16))
Vol. heat capacity of solid $\rho_s c_s$	[MJ m^{-3} K^{-1}]	2.06 ± 0.02	according to Eq. (1)
Thermal conductivity of solid λ_s	[W m^{-1} K^{-1}]	3.2 ± 0.2	measured (modified transient plane source)
Thermal effusivity of solid e_s	[J K^{-1} m^{-2} s$^{-1/2}$]	2584 ± 93	measured (modified transient plane source)
Thermal conductivity of fluid λ_f (20 °C)	[W m^{-1} K^{-1}]	0.598	taken from literature (VDI, 2013)
Thermal conductivity of sat. porous media λ_b	[W m^{-1} K^{-1}]	1.75	according to Eq. (3)
Vol. heat capacity of fluid $\rho_f c_f$ (20 °C)	[MJ m^{-3} K^{-1}]	4.18	taken from literature (VDI, 2013)
Vol. heat capacity of sat. porous media $\rho_b c_b$	[MJ m^{-3} K^{-1}]	2.87 ± 0.02	according to Eq. (2)
Resulting R_{app}	[–]	1.88	according to Eq. (5)

2.1.4. Experimental preparation

The column was set up vertically for the filling procedure. The gravel was packed in the column in layers of approximately 5 cm from bottom to top. Each layer was compacted by mechanical force using a metal plate. The Pt100 sensors were installed during the column packing by inserting the sensors through fittings into the column. A thin, perforated aluminum plate was placed on top of the gravel after filling. This plate was attached to the lid by threaded rods, allowing it to be moved in a vertical direction. This prevented the gravel from shifting during the tilting of the column. To establish a uniform initial temperature, the column was injected with water until a uniform temperature was reached at all temperature sensors.

Prior to the start of the experiment, the three-way valves close to the inflow were adjusted to block the inflow to the column and to dispose the water. This was done to ensure that the water in the inflow tubes was the same temperature as the inflow temperature. As this was established, the three-way valves were adjusted to enable inflow into the column.

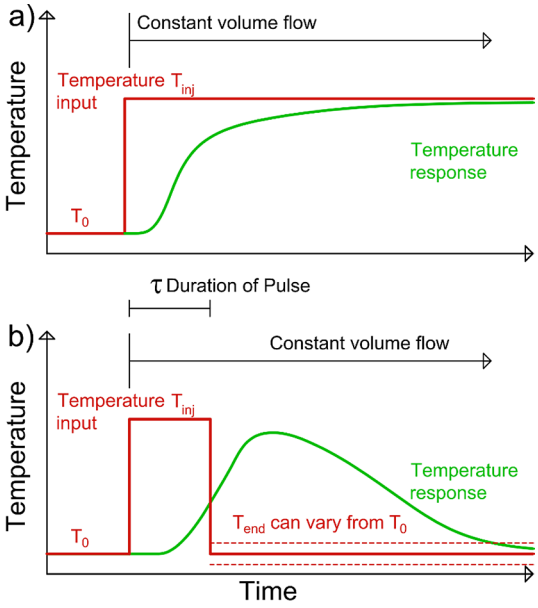

Fig. 2. Experimental procedures for (a) step input and (b) finite duration pulse experiments.

2.1.5. Experimental procedure

Two different experimental setups, step input and finite duration pulse, were used to evaluate which methods can be used to determine the advective thermal velocity for estimation of the apparent retardation factor, R_{app}. For the step input experiments (Fig. 2a), the column was positioned vertically and the injection and flow of the water was from top to bottom. The initial temperature was set to $T_0 = 10\,^{\circ}C$. The water from the water tap flowed through both heat exchangers into one tank of the second thermostat. When the temperature in the tubes reached T_{inj}, the three-way valves were adjusted to start the injection of the tempered water into the column. This step was defined as the experimental start time ($t = 0$). The injection temperatures were either set to 30 °C or 15 °C, to evaluate any influence of different injection temperatures. The experiments were stopped when the center temperature sensor most distant from the inflow reached a constant value close to T_{inj}.

The second setup was a finite duration pulse (Fig. 2b). A heat pulse was created by injecting hot water (T_{inj}) for a defined time τ into the column. The pulse time τ was 30 min for all experiments. This value was chosen, as it allows a sufficiently measurable temperature signal. Furthermore, it does not significantly affect the results. This was investigated prior to the experiments using Eq. (13) with varying values of τ and v_a. When $t = \tau$ was reached, the injection temperature was changed back to T_0. In a first series of experiments, a vertical setup was used. However, in these experiments the temperature BTCs were influenced by free convection even at temperature differences between T_{inj} and T_0 smaller than 5 K (see supplement Fig. S1).

Free convection can occur due to thermally induced density differences of the water. Some studies concluded that density effects can be neglected, if the temperature difference is lower than 15 °C (Lo Russo & Taddia 2010, Ma and Zheng 2010). Nagano et al. (2002) investigated the influence of natural convection on forced horizontal flow experimentally. They developed a criterion based on the *Reynolds number* and the modified Rayleigh number under which natural convection exerts an obvious influence for a system of forced flow. According to this criterion, which depends among other parameters on the permeability, the kinematic viscosity, particle diameter and temperature difference, the experiments should not be influenced by free convection. Schincariol and Schwartz (1990) concluded in an experimental study that buoyancy effects occur at density difference higher than $0.8\,kg\,m^{-3}$. Due to the nonlinear dependency of the water density on temperature, density effects can occur at lower temperature differences if the absolute temperature is higher. The used temperatures of 20 °C initial temperature and 25 °C injection temperature lead to density differences of $1.16\,kg\,m^{-3}$ which would explain the observed effects according to the findings of Schincariol and Schwartz (1990). Density driven free convection has also been observed in a field experiment with temperature differences of 8 °C (ambient temperature 17 °C injection temperature 9 °C) and advection dominated conditions (Ma et al., 2012). Therefore, density effects should be accounted for if heat is used as a tracer, keeping in mind the nonlinear dependency of the water density on temperature.

Due to the potential influence of free convection, the finite duration pulse experiments in a vertical setup were not used further in the investigation. Instead, the experiments for the finite duration pulse were executed in a horizontal setup to minimize free convection effects. In the horizontal setup, the free convection is not acting in the same direction as the forced convection. The finite duration pulse was carried out by setting one of the thermostats to the injection temperature T_{inj}. The other thermostat was set to the initial temperature T_0. When the temperature in the inflow tubes reached T_{inj}, the three-way valves were adjusted to start the injection into the column. Again, this was the experimental start time ($t = 0$). When t was equal to τ, the injection temperature was set back to the initial temperature by changing the inflow from the first thermostat (T_{inj}) to the other thermostat (T_0). Due to varying ambient temperatures, and despite thermal insulation of the tubes from the thermostats to the column, the measured injection temperature after the pulse (T_{end}) did not always exactly match the initial temperature. This means that T_{end} varied slightly (maximally by 0.1 of normalized temperature) from T0 (Fig. 2b). To minimize the free convection in the horizontal setup, reduced temperature differences were used. The injection temperature T_{inj} was set to 25 °C and the initial and end temperature to 20 °C. The experiments were stopped when the center temperature sensor most distant from the inflow reached a constant value near T_{end}. The experiment duration varied depending on the volume flow between 3 h and > 15 h. Altogether, 43 experiments were conducted, as summarized in Table 3.

Table 3
Details of the conducted experiments. The experiment duration varied between 3 h and > 15 h depending on the volume flow. The duration of the pulse τ was 30 min for all finite duration pulse experiments. *The finite duration pulse experiments in vertical direction were not used in the analysis due to the observed influence of free convection.

Experiments	Finite duration pulse		Step input
Seepage velocities	~6–34 m/d		~5–50 m/d
Setup	vertical	horizontal	Vertical
Flow direction	top to bottom	left to right = bottom to top (but horizontal)	top to bottom
Initial temperature	~15–20 °C	~20 °C	~10 °C
Input temperature	~25 °C	~25 °C	~15 °C / ~30 °C
Number of heat experiments	8*	11	14
Coupled heat and solute experiments	–	8	2

In the coupled heat and solute tracer experiments, the three-way valve at each inflow tube was employed to inject 2 ml of a $10^{-5}\,kg\,L^{-1}$ uranine solution, resulting in a total injected mass of 0.16 mg uranine per experiment. Uranine is a suitable solute tracer for this setting, as it has been proven to be thermally very stable (Adams and Davis, 1991) and the temperature dependency of the intensity for the maximum expected temperature difference of 10 °C is less than 5% (Smart and Laidlaw, 1977; Leibundgut et al., 2009). In the step input experiments, the solute tracer was injected simultaneously with the start of the hot

water injection ($t_{sol\ inj} = 0$). In the finite duration pulse experiments, the uranine was injected when 50% of the heat pulse was reached ($t_{sol\ inj} = 0.5\tau$). The samples were taken at the outflow of the column in varying time intervals depending on the applied volume flow.

2.2. Evaluation of thermal and solute breakthrough curves

To evaluate possible LTNE effects, the measured, effective thermal retardation (Eq. (4)) which is potentially influenced by LTNE effects, is compared with the predicted, apparent thermal retardation (Eq. (5)) which assumes LTE:

$$R_{eff} = \frac{v_a}{v_{therm}} \tag{4}$$

where v_{therm} is the mean velocity of the thermal front. The effective fluid or seepage velocity v_a is defined as $v_a = \frac{q}{n_{eff}}$, with the specific discharge q and the effective porosity n_{eff}. The specific discharge is defined as $q = \frac{Q}{A}$, with the volume flow Q and the cross-sectional area A. The predicted, apparent thermal retardation factor is defined by:

$$R_{app} = \frac{\rho_b c_b}{n_{tot}\rho_f c_f} = 1 + \frac{(1 - n_{tot})\rho_s c_s}{n_{tot}\rho_f c_f} \tag{5}$$

where $\rho_{f,s,b}$ is the specific density of the fluid, solid or bulk porous media, $c_{f,s,b}$ is the specific heat capacity of the fluid, solid or bulk porous media, and n_{tot} is the total porosity.

The relative contributions of convective to conductive heat flow can be expressed by the thermal Péclet number (e.g. De Marsily 1986):

$$Pe = \frac{\rho_f c_f q L}{\lambda_b} \tag{6}$$

where ρ is the specific density, c is the specific heat capacity, λ is the thermal conductivity with the subscripts s, f and b denoting the corresponding value for the solid, fluid or the bulk stagnant saturated porous media, and L is the characteristic length, usually set to the mean particle diameter (Rau et al., 2014).

2.2.1. Thermal breakthrough curves

In the step input experiments, five thermal velocities were calculated for each sensor and experiment by:

$$v_{therm} = \frac{distance_{Pt100}}{t_{char}} \tag{7}$$

with $distance_{Pt100}$ as the distance of the temperature sensor from the inflow. The characteristic time t_{char} for $v_{therm\ T25}$, $v_{therm\ T50}$ and $v_{therm\ T75}$ is defined as the time when the normalized temperature reached 25%, 50%, 75%, respectively. The t_{char} for $v_{therm\ peak\ dT/dt}$ is defined as the time, when the first time derivative of the thermal BTC reaches its maximum. The t_{char} for the peak velocity in the finite duration pulse experiments is the time when the maximum temperature of the thermal BTC for each sensor is reached. These or similar approaches are common to determine the thermal velocity from thermal BTCs (Table 1) and were therefore chosen in this study.

Moreover, an analytical model for each setup was used to determine the longitudinal effective thermal dispersion coefficient D_l (Eq. (8)) (De Marsily, 1986) and the thermal velocity $v_{thermfit}$:

$$D_l = \kappa_b + \alpha_l^t \left|\frac{\rho_f c_f}{\rho_b c_b} q\right| = \frac{\lambda_b}{\rho_b c_b} + \alpha_l^t \left|\frac{\rho_f c_f}{\rho_b c_b} q\right| \tag{8}$$

where κ_b is the stagnant thermal diffusivity of the saturated porous medium, $\alpha_l^t \left|\frac{\rho_f c_f}{\rho_b c_b} q\right|$ is the thermal mechanical dispersion, and α_l^t is the thermal dispersivity.

2.2.1.1. Analytical solution - step input. An analytical solution is used to derive the thermal velocity and the longitudinal effective thermal dispersion from the thermal BTC. The solution of the 1D convective dispersive heat transport equation for a step input is given by Eq. (9) (van Genuchten and Alves, 1982; Runkel, 1996) and Eq. (10) with the boundary and initial conditions listed in Eq. (11a) and (11b), respectively:

$$G_{x,t} = \left[\frac{1}{2} erfc\left(\frac{x - v_{thermfit} t}{2\sqrt{D_l t}}\right) + \sqrt{\frac{{v_{thermfit}}^2 t}{\pi D_l}} exp\left[-\frac{(x - v_{thermfit} t)^2}{4 D_l t}\right] - \frac{1}{2}\left(1 + \frac{v_{thermfit} x}{D_l} + \frac{{v_{thermfit}}^2 t}{D_l}\right) exp\left(\frac{v_{thermfit} x}{D_l}\right) erfc\left(\frac{x + v_{thermfit} t}{2\sqrt{D_l t}}\right)\right] \tag{9}$$

$$T_{(x,t)} = T_0 + (T_{inj} - T_0) G_{x,t} \tag{10}$$

$$T_{(x,0)} = T_0 \tag{11a}$$

$$T_{(0,t)} = T_{inj} \tag{11b}$$

where D_l is the longitudinal effective thermal dispersion coefficient and $v_{thermfit}$ is the thermal velocity, t is the time, x is the distance, T_{inj} is the injection temperature and T_0 is the initial temperature.

2.2.1.2. Analytical solution - multiple pulse input. As described in Section 2.1.5, due to varying ambient temperatures and despite the thermal insulation of the tubes from the thermostats to the column, the initial temperature did not always exactly match after the end of the pulse duration. For this reason, the analytical solution for a multiple pulse input boundary condition was used instead of a solution for a finite duration pulse. The analytical solution for multiple pulse input conditions can be written as the sum of the solutions for the individual pulses (Eq. (12)) (van Genuchten and Alves, 1982; Toride et al., 1995). This results in Eq. (13) for the multiple pulse input conditions (Eq. (14a), b, c) applied in the present study:

$$T_{(x,t)} = \sum_{j=1}^{i} (T_{j,0} - T_{j-1,0}) G_{(x,t-\tau_{i-1})} \tag{12}$$

$$T_{(x,t)} = \begin{cases} t \le \tau;\ T_0 + (T_{inj} - T_0) G_{(x,t)} \\ t > \tau;\ T_0 + (T_{inj} - T_0) G_{(x,t)} + (T_{end} - T_{inj}) G_{(x,t-\tau)} \end{cases} \tag{13}$$

$$T_{(x,0)} = T_0 \quad \text{for } x \ge 0 \tag{14a}$$

$$T_{(0,t)} = T_{inj} \quad \text{for } \tau \ge t \ge 0 \tag{14b}$$

$$T_{(0,\infty)} = T_{end} \quad \text{for } t > \tau \tag{14c}$$

where τ_i represents the duration of the pulse i, x is the distance, t is the time, T_{inj} is the injection temperature, and T_0 is the initial temperature. The normalized versions of Eqs. (10) and (13) were used to determine the longitudinal effective thermal dispersion, D_l, and to fit the thermal velocity, $v_{therm\ fit}$. This was done by minimizing the sum of squared differences between the normalized measured temperatures and the normalized modeled temperatures for each sensor with the corresponding distance, x.

2.2.2. Solute breakthrough curve

To determine the hydrodynamic flow conditions and parameters of the experiments, the recorded solute BTCs were examined. The analytical solution to the 1D advection dispersion model for an instantaneous injection is given by Lenda and Zuber (1970), Eq. (15) based on Eqs. (16) and (17), given the initial and boundary conditions listed as Eqs. (18a, b, c):

$$C(t) = \frac{M}{Q t_0} \frac{1}{\sqrt{4\pi P_D (\frac{t}{t_0})^3}} \exp\left[-\frac{\left(1 - \frac{t}{t_0}\right)^2}{4 P_D \frac{t}{t_0}}\right] \tag{15}$$

$$n_{eff} = \frac{Qt_0}{\pi r^2 x} \tag{16}$$

$$\alpha_l^s = xP_D \tag{17}$$

$$C_{(x,0)} = \frac{M}{Q}\delta(t) \quad \text{for} \quad x \geq 0 \tag{18a}$$

$$C_{(0,0)} = 0 \tag{18b}$$

$$\lim_{x\to\infty} C_{(x,\infty)} = 0 \tag{18c}$$

where α_l^s is the solute longitudinal dispersivity, Q is the volume flow, r is the radius of the column, M the injected tracer mass, t_0 is the mean transit time and P_D is the dispersion parameter. The values of t_0 and P_D were determined by least-square based fitting of Eq. (15) to the measured solute BTC. The seepage velocity is determined via $v_a = \frac{x}{t_0}$, where x is the distance between injection and the sample point, which here is equal to the length of the column (1.5 m).

3. Results and discussion

3.1. Solute transport experiments

The solute tracer experiments were carried out to examine the correlation between the seepage velocity (mean solute velocity) v_a, the volume flow Q and the effective porosity n_{eff} of the porous media (Table 4). The tracer mass recovery was calculated as given in Klotz et al. (1988). The high tracer mass recoveries indicate that most of the tracer mass was successfully injected into the column, and sorption or degradation did not take place at a significant amount. The loss in tracer mass could be due to stopping the measurements too early, photolytic degradation or trapping of small amounts of the tracer in the injection valve.

The analytical model in Eq. (15) successfully reproduces the solute BTCs from the laboratory measurements at all volume flows (see supplement Fig. S2). As expected, the determined values of v_a showed a linear dependency on Q. A linear regression (through origin) was applied to predict the values of v_a based on the applied volume flow for the "heat only" experiments (see supplement Fig. S3). The regression curve based on the analytical modeling results matches well with the corresponding v_a calculated by the specific discharge. The regression from the velocities determined with the analytical model from the solute BTCs show nearly the same slope as the expected value from the Darcy flux. This indicates that the flow through the column was nearly uniform with negligible effects of wall flow or preferential flow paths.

3.2. Heat transport experiments

3.2.1. Comparison of thermal velocities for step input scenarios

The effective thermal retardation in the step input experiments demonstrates good agreement with the apparent thermal retardation for $v_{therm\ fit}$ and $v_{therm\ T50}$ indicating that LTNE effects do not significantly influence the derived thermal velocity. An example of the thermal BTCs of the center temperature sensors from a step input experiment are shown in Fig. 3. The black lines indicate the modeled temperatures for each sensor, whereas the colored lines show the measured temperatures. The modeled temperatures from the analytical solution fit well with the measured temperatures for all step input experiments. With rising distance from the inflow, the differences between measured and modeled temperatures increase at the end of the BTCs (max. 0.08 of normalized temperature as highest deviation of all experiments). We interpret this as being due to slight heat loss from the column due to lower room temperatures.

The thermal BTCs of the off-center temperature sensors were used to check for uniform flow through the column. Fig. 4 shows the thermal BTCs of different vertical profiles, at ± 8 cm from the center (Fig. 1), at 10 cm and 30 cm (top-to-bottom experiment (a)) and 110 cm and 130 cm (bottom-to-top experiment (b)). The bottom-to-top experiment was carried out to check for uniform flow in close proximity to the inflow area. The off-center temperature sensors delineate a nearly simultaneous increase with the temperature of the center locations. The + 8 cm sensors show a slightly faster increase. The mostly simultaneous rise of the temperature indicates that a uniform flow through the column was achieved.

The effective thermal retardation factors, R_{eff} obtained by (Eq. (4)) for the different experiments are shown in Fig. 5a. The corresponding apparent retardation factor, R_{app} (Eq. (5)) determined for the different thermal velocities in relation to the seepage velocity is 1.88. The normalized deviation of R_{eff} from R_{app} is shown in Fig. 5b. While $v_{therm\ T25}$ and $v_{therm\ peak\ dT/dt}$ generally deliver lower values of R_{eff} than of R_{app}, $v_{therm\ T75}$ yields higher values. The deviations increase at seepage velocities lower than around 10 m d^{-1}. However, the discrepancy between R_{eff} and R_{app} were small for $v_{therm\ fit}$ and $v_{therm\ T50}$ for all investigated velocities. These systematic deviations between R_{eff} and R_{app} for the different calculation procedures result in systematic deviations in the derived flow velocities or heat capacities (Table 5), if the thermal velocities are used with R_{app} (Eq. (5)).

The absolute values of R_{eff} and deviations from R_{app} for the different thermal velocities vary among the experiments and show scatter. These variations cannot be explained by non-ideal input conditions, as the influence of non-uniform boundary conditions in laboratory soil columns should dissipate at 3/2 of the radius of the column (Barry, 2009), meaning for this setup at distances higher than 21.75 cm. The relative differences between the thermal velocities are quite constant. Fig. 6 shows the normalized deviation from $v_{therm\ fit}$ for each thermal velocity and in relation to the seepage velocity. The value of $v_{therm\ fit}$ is chosen as the reference velocity. Obviously, these fitted values can be seen as the most reliable to estimate the thermal velocity as the analytical model accounts for both advective and dispersive conductive heat transport. For seepage velocities > ~10 m d^{-1} the deviations from $v_{therm\ fit}$ are quite constant, with around 10% overestimation of the seepage velocity for $v_{therm\ T25}$ and 10–15% underestimation for $v_{therm\ T75}$. At lower flow velocities, the differences from $v_{therm\ fit}$ rise, especially for $v_{therm\ T25}$ and $v_{therm\ T75}$. The $v_{therm\ peak\ dT/dt}$ vary between $v_{therm\ fit}$ and $v_{therm\ T25}$, and exhibit the highest variability among one (Fig. 5) and also all experiments (Fig. 6).

The constant relative differences of the determined thermal velocities from $v_{therm\ fit}$ (Fig. 6) indicate that the scatter in R_{eff} (see Fig. 5a) could also be caused by the experimental setup. A possible explanation could be the occurrence of wall flow in some of the experiments. Wall flow could lead to an overestimation of the seepage velocity in the center of the column. Other studies (such as Bandai et al., 2017), using a column with saturated porous media to investigate heat and solute dispersivities experienced the occurrence of wall flow, but it was considered negligible. Another explanation could be non-uniform heat flow due to the large grain sizes. Rau et al. (2012b) observed non-uniform heat flow due to preferential flow paths in 1D tank experiments with grain sizes of 2 mm and hypothesized that these effects could be considerably more significant in sediments with larger grain sizes. However, as these variations are relatively small compared to the total deviations of R_{eff} from R_{app}, this is not considered as a relevant bias for the results here.

Table 4
Measured and calculated parameters derived from the solute tracer tests.

Parameter	n_{eff} [–]	Tracer mass recovery [–]	Longitudinal solute dispersivity [mm]
Mean	0.35	0.92	38
Standard deviation	0.02	0.08	5

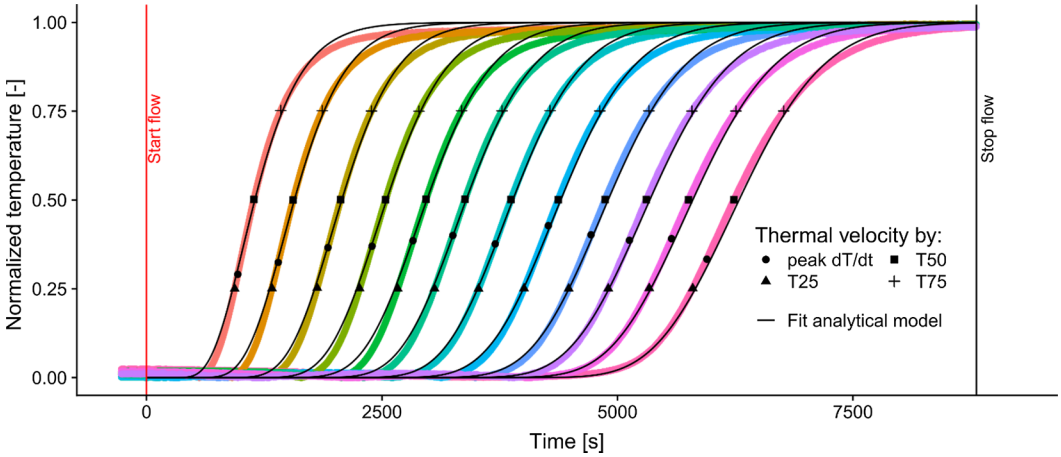

Fig. 3. Example of the thermal BTCs of a step input experiment with a seepage velocity of 37 m d^{-1}. The colored lines show the measured temperatures with each color indicating a different distance from the inflow. The black lines are derived by the fitted model for each sensor. (For interpretation of the references to color in this figure legend, the reader is referred to the web version of this article.)

In this study, the thermal velocity determined with the analytical model results in a good agreement between R_{eff} and R_{app} for all investigated flow velocities. As a comparison, in the experiments of Rau et al. (2012a), the fluid velocities derived from the thermal BTCs with an analytical model demonstrated a systematic overestimation of the solute derived velocities by approximately 20%, which was explained by spatial heterogeneities. Another reason for their systematic overestimation could be the occurrence of LTNE effects. As discussed in Rau et al. (2014), the LTE assumption might be flawed in natural materials in the Darcy range. Our results showed a reasonably good agreement between the expected and effective thermal retardation. Hence, if LTNE effects occur within the investigated porous medium of our experiment, they are masked by the scatter in the effective thermal retardation possibly caused by non-uniform flow induced by the large grain sizes or the laboratory setup. This means that LTNE effects, if they occur within the examined experimental conditions, do not significantly influence the resulting thermal velocity determined by fitting the analytical solution to the thermal BTCs of the step input experiments. But LTNE effects could influence thermal mechanical thermal dispersion, as Bandai et al. (2017) showed that effective thermal dispersion is particle-size dependent, while solute dispersion is not. Fig. 7 depicts the summary of the effective thermal dispersion coefficients of the step input experiments of our study compared with the data from Bandai et al. (2017). This comparison confirms the dependency of the normalized thermal dispersion coefficient on the grain size. Smaller grain sizes appear to lead to higher normalized dispersion coefficients for the same Péclet number.

As argued by Rau et al. (2012b), non-uniform flow could introduce lateral heat fluxes, which are violating the 1D assumption of the analytical model. This could also cause different longitudinal thermal dispersion values derived from the 1D analytical model.

The effective thermal retardation factor R_{eff} for the thermal velocity $v_{therm\ T50}$ matches the expected R_{app}. This is in agreement with the results of the numerical study of Irvine et al. (2013), where solute and heat derived velocities from the mean value between injection and initial temperature/concentration showed little deviation. This demonstrates that the thermal velocity determined by the mean between the injection and initial temperature is mainly influenced by advection. The difference between thermal conduction and solute diffusion and the differences in solute and heat mechanical dispersion obviously have no relevant effect on this thermal velocity ($v_{therm\ T50}$) for the range of flow velocities investigated in the present experiment.

The thermal velocities from $v_{therm\ T25}$, $v_{therm\ T75}$ and $v_{therm\ peak\ dT/dt}$ show systematical deviations between R_{eff} and R_{app}. These velocities are therefore influenced by thermal dispersion. Using these velocities with R_{app} to derive the seepage velocity or heat capacities (Eqs. (4) and (5)) results in erroneous values. However, as the measured deviations were nearly constant at seepage velocities higher than 10 m d^{-1}, these deviations could be compensated by applying a correction factor (here around 0.86 for $v_{therm\ T75}$ and 1.11 for $v_{therm\ T25}$, see Fig. 6) if the

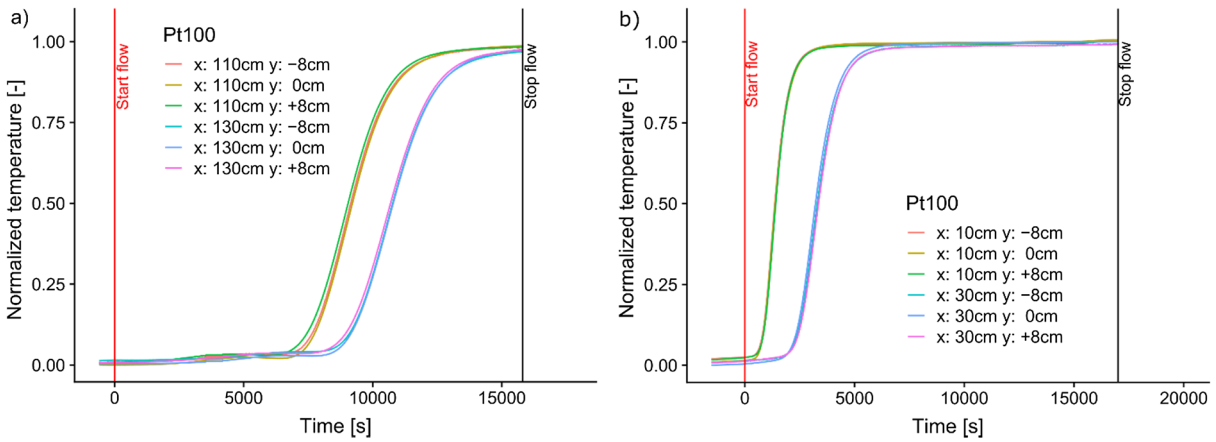

Fig. 4. Thermal BTCs for the lateral positions ± 8 cm from the center and center sensors showing similar behavior and indicating mostly uniform flow through the column; a) illustrates the BTCs in a top-to-bottom setup, with the sensors at + 8 cm showing a slightly faster increase; b) depicts the thermal BTCs for a bottom-to-top experiment.

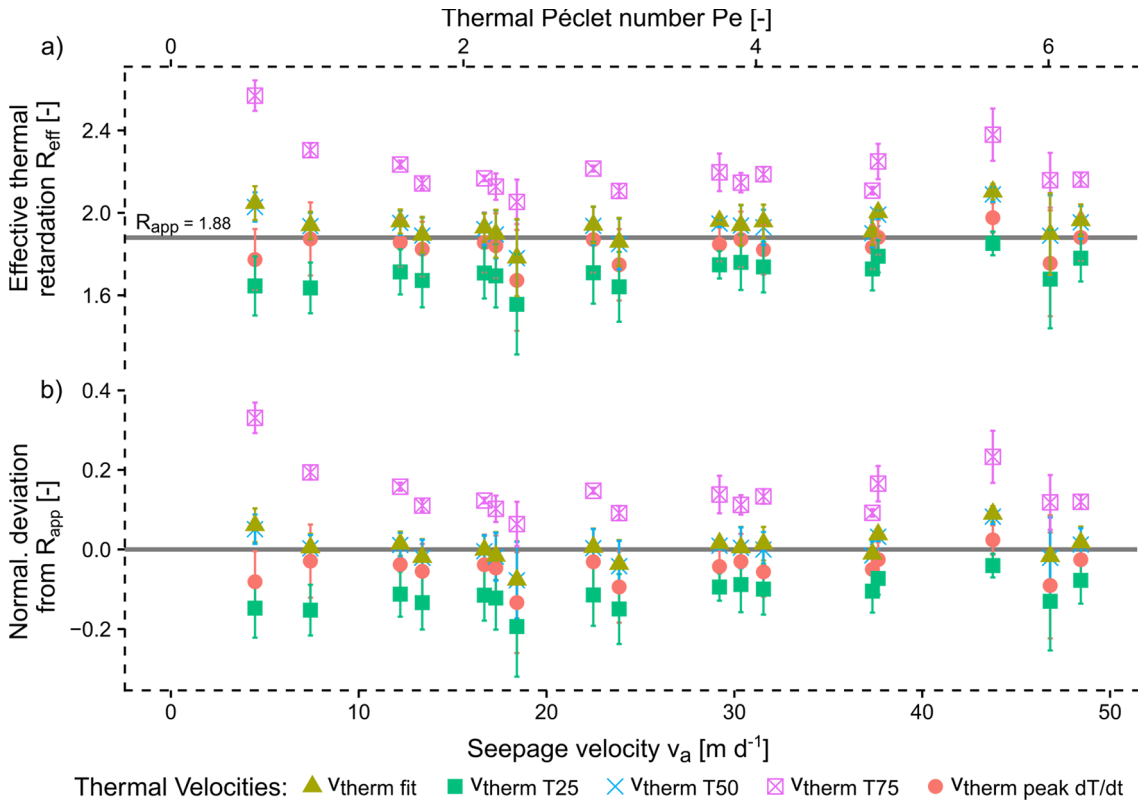

Fig. 5. (a) Determined effective thermal retardation calculated by Eq. (4) from the measured thermal velocities and flow velocities for all step input experiments. The apparent thermal retardation of 1.88 calculated by Eq. (5) from the heat capacities and total porosity is shown as the gray line. (b). shows the normalized deviation from R_{app}. The error bars indicate the standard deviation when all distances are compared in one experiment.

Table 5
Overview of the deviations between the apparent thermal retardation R_{app} and the effective thermal retardation R_{eff} for the step input experiments and the resulting consequences if these thermal velocities are used to infer flow velocities or heat capacities.

Thermal velocity	R_{eff} vs. R_{app}	Mean deviation [%]	Impact on evaluation if v_{therm} is used to infer seepage velocities/heat capacities.
$v_{therm\ T25}$	$R_{eff} < R_{app}$	−11.1	Overestimation of seepage velocities / underestimation of heat capacity of porous media; deviation increases with lower seepage velocities (< 10 m/d).
$v_{therm\ T75}$	$R_{eff} > R_{app}$	14.1	Underestimation of seepage velocities / overestimation of heat capacity of porous media; deviation increases with lower seepage velocities (< 10 m/d).
$v_{therm\ peak\ dT/dt}$	$R_{eff} \sim < R_{app}$	−4.3	Overestimation of seepage velocities / underestimation of heat capacity of porous media.
$v_{therm\ fit}$	$R_{eff} \sim R_{app}$	−0.7	Can be used to infer seepage velocities and heat capacity.
$v_{therm\ T50}$	$R_{eff} \sim R_{app}$	−0.2	

deviations are known or determined by prior experiments. Such an approach was used by Somogyvári and Bayer (2017) to reduce the measurement time of thermal BTCs in a field experiment to reconstruct aquifer heterogeneity with a thermal tracer test in a tomographic setup.

3.2.2. Comparison of thermal velocities for finite duration pulse scenarios

The finite duration pulse experiments were conducted to evaluate if the peak velocity in a finite duration pulse heat tracer setup can be used to infer the seepage velocity and involved bulk heat capacity. At seepage velocities higher than 10 m d^{-1}, the effective thermal retardation for the peak velocity and the fitted velocity demonstrates good agreement with the apparent thermal retardation. At seepage velocities lower than 10 m d^{-1}, the effective thermal retardation is lower than expected for the peak velocity (Fig. 10).

Fig. 8 shows the thermal BTCs for a finite duration pulse experiment. The highest pulse temperature is reached at the first temperature sensor at a distance of 10 cm from the inflow. With increasing distance, the pulse temperature decreases and the BTCs spread. The modeled values show the best fitted temperatures from the analytical model (Eq. (13)). While in the step input scenario, the fit of the analytical model is very good, the analytical model in the finite duration pulse scenarios is not able to match the observed temperatures at all distances and experiments. This could be caused by the temperature differences in vertical direction, which developed in the experiment shortly after the inflow (Fig. 9). With increasing distance from the inflow, the differences in temperatures increased. Nevertheless, the peak velocities are similar and as the solute tracer tests showed homogenous flow, we consider the peak velocities as unbiased. As normalization of the temperature was done with the injection temperature and initial temperature, negative normalized temperatures can occur (Fig. 9) when the end temperature T_{end} differed from the initial temperature T_0. As explained in Section 2.1.5 this did occur to a lesser extent in some of the experiments due to varying room temperatures.

Fig. 10 shows the effective thermal retardation R_{eff} for all finite duration pulse experiments, if the thermal velocity is determined by either the peak velocity or an analytical model (Eq. (13)). For higher seepage velocities, values of R_{eff} determined with the peak and analytical model are in the range of the apparent retardation R_{app}. At seepage velocities lower than 10 m d^{-1}, R_{eff} referring to the thermal peak velocities generally decreases, reaching values of less than 30% lower

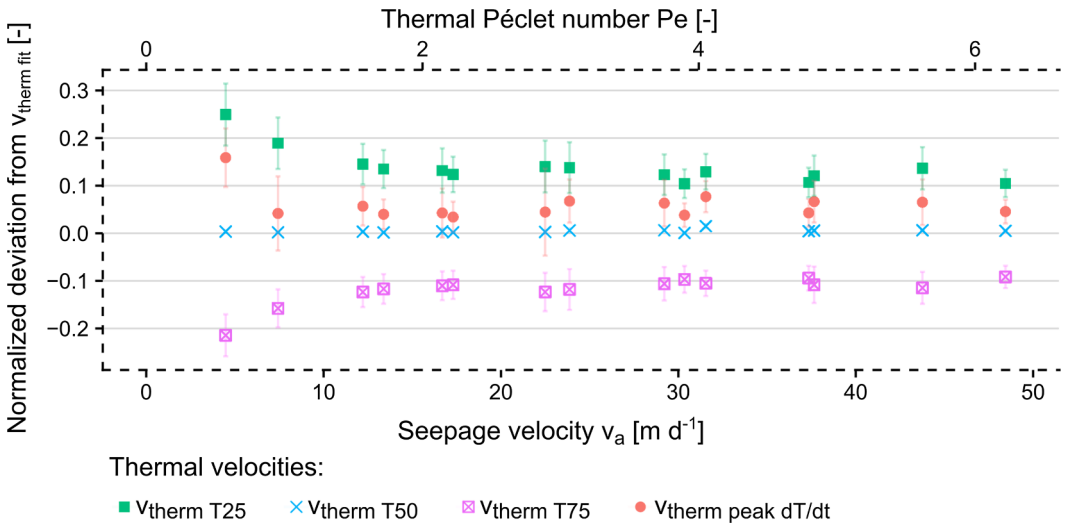

Fig. 6. Normalized deviation from the thermal velocity determined by the analytical model ($v_{therm\ fit}$) of the different v_{therm} for the step input experiments. The error bars indicate the standard deviation for the velocity of all distances.

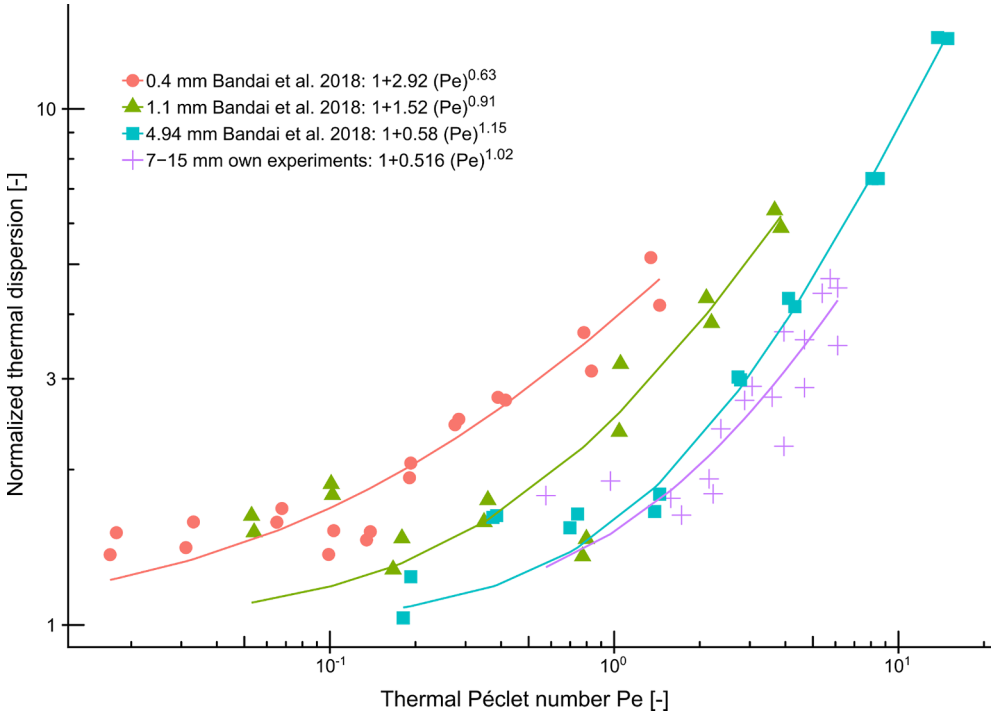

Fig. 7. Comparison of the normalized thermal dispersion coefficient $\boldsymbol{D_l/\kappa_b}$ for different grain sizes with data from (Bandai et al., 2017). The values for the best fit for the power law equation between normalized thermal dispersion and thermal Péclet number (Eq. (6)) as suggested by Metzger et al. (2004) & Bandai et al. (2017) is shown in the legend.

than $R_{app.}$ This demonstrates that the peak velocity does not represent a purely advective velocity. As heat losses would lead to a delayed peak arrival time (Pan et al., 2019), the peak velocity is influenced by conduction at seepage velocities lower than 10 m d^{-1} for the investigated porous medium. One experiment with a seepage velocity of around 6.3 m d^{-1} deviates from this behavior (gray triangle in Fig. 10). This experiment is considered as an outlier, and a possible explanation could be an error in the determination of the volume flow. The measured R_{eff} for the thermal velocity determined by the analytical model showed lower deviations from R_{app}. Nevertheless, the overall deviation of R_{eff} is clearly higher than in the step input experiments (Fig. 10). A possible reason for this is the influence of the free convection in the horizontal experiments. The boundary conditions of the analytical solution would be violated by the temperature differences induced by free convection.

Similar results, that the peak velocity was overestimating the thermal velocity compared to the velocity derived from an analytical model in slow flow conditions (~8.1 m d^{-1}), were found by Becker et al. (2013). They used fiber optic distributed temperature sensing to measure infiltration rates in a recharge basin. A good agreement between thermal peak transit times and solute tracer transit times was reported by Becker et al. (2015), who employed peaks of diurnal temperature signals and bromide and B^{10}-enriched boric acid in a managed aquifer recharge system to determine mean transit times. However, flow velocities were not determined. The deviations of R_{eff} for the peak velocity from R_{app} at lower seepage velocities can most likely be explained by the influence of thermal conduction on the thermal peak

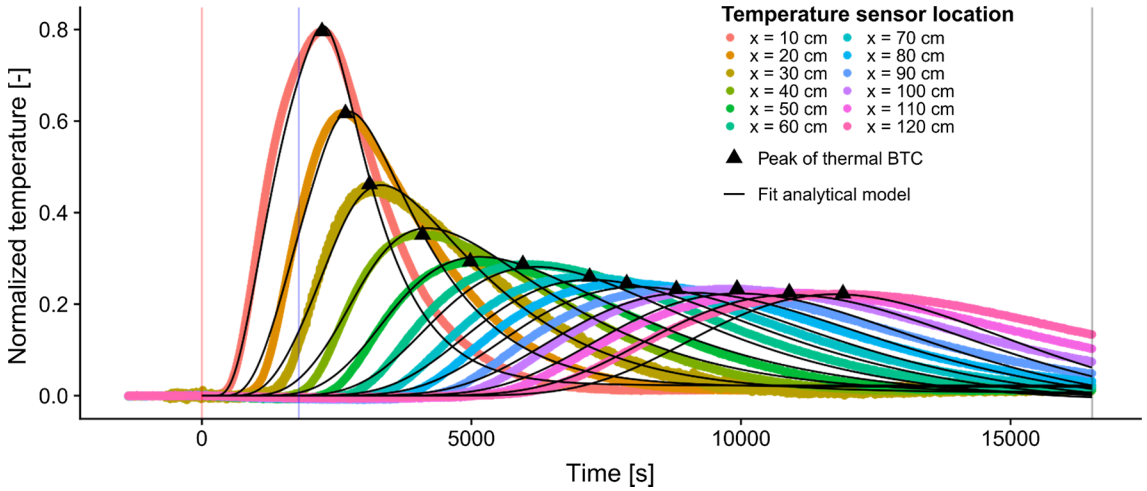

Fig. 8. Thermal BTCs and fit of the analytical model of a finite duration pulse experiment with a seepage velocity of 20.2 m d^{-1}. The colored lines are the measured temperatures for the center temperature sensors in different distances to the inflow. The vertical red, blue and gray line indicate the start of the pulse, the end of the pulse and the stop of the volume flow, respectively. (For interpretation of the references to color in this figure legend, the reader is referred to the web version of this article.)

velocity. With decreasing flow velocities, the influence of thermal conductivity increases as expressed by the thermal Péclet number (Eq. (6)).

4. Conclusions

This study systematically compared the apparent thermal retardation R_{app} with the effective thermal retardation R_{eff} to evaluate possible influences of LTNE effects on the heat transport in conditions of a highly permeable porous aquifer. Furthermore, different methods to determine the advective thermal velocity were evaluated. This is needed to correctly use the thermal retardation factor to derive the seepage velocity or bulk heat capacity from thermal BTCs. Overall, 43 one-dimensional heat and coupled heat and solute tracer tests with a step input scenario and a finite duration pulse input scenario were conducted in laboratory experiments, using a gravel filled column.

The results show that when a step input signal is interpreted, the thermal velocities determined by an analytical model or the mean between the injection and the initial temperature can be used with R_{app} to predict the seepage velocities or bulk heat capacity of the porous medium in one-dimensional settings. These findings also reveal that LTNE effects do not remarkable influence the resulting thermal velocities from these two methods. However, the normalized thermal dispersion coefficient seems to be dependent on particle size, which could be governed by LTNE.

In the step input experiments, the effective thermal retardation of thermal velocities derived by the peak of the first time derivative or self-defined values between injection and initial temperatures (e.g. $v_{therm\ T25}/v_{therm\ T75}$) deviate from R_{app} because these velocities are not strictly advective and influenced by the thermal dispersion coefficient. The effective thermal retardation by these methods shows a systematical deviation of 10–15% from R_{app}. However, the results suggest that these deviations are nearly constant at seepage velocities higher than 10 m d^{-1}, and that these deviations could be compensated by applying a correction factor (here ca. 0.86 for $v_{therm\ T75}$ and 1.11 for $v_{therm\ T25}$) if the deviations are known or determined by prior experiments. This would allow reduction of the measurement time in future thermal tracer tests, since the complete thermal BTC is not needed for evaluation.

The peak velocity appears to be significantly faster than predicted by R_{app} in cases with seepage velocities lower than 10 m d^{-1} leading to higher thermal velocities and an overestimation of the seepage velocity

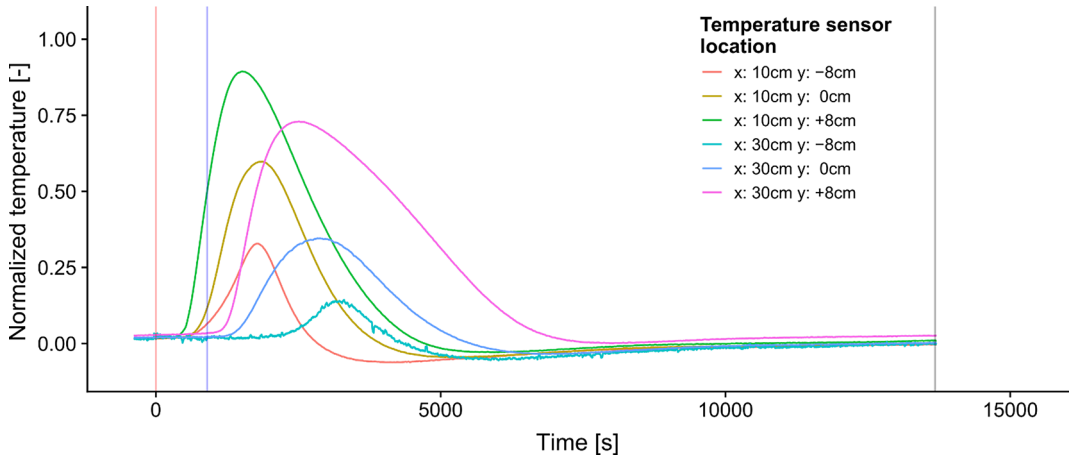

Fig. 9. Thermal BTCs for the lateral positions ± 8 cm from the center at 10 cm and 30 cm after inflow for a finite duration pulse experiment with a seepage velocity of 22 m d^{-1}. The temperature sensors at the top position (+8cm) show the highest temperatures, and the bottom sensors (-8 cm) show the lowest temperature during the pulse. The vertical red and blue line indicate the start and stop of the temperature pulse. (For interpretation of the references to color in this figure legend, the reader is referred to the web version of this article.)

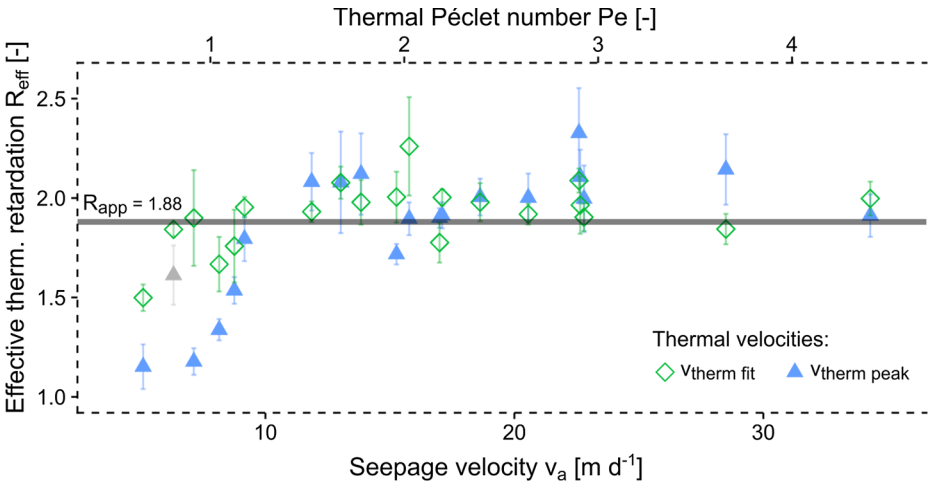

Fig. 10. Influence of the seepage velocity on effective thermal retardation (v_a/v_{therm}) for the horizontal finite duration pulse experiments. The thermal velocity is either determined as fitting parameter of an analytical model (Eq. (13)) or as the peak velocity. The apparent thermal retardation of 1.88 calculated by Eq. (5) from the heat capacities and total porosity is shown as the gray line. The error bars represent the standard deviation for the velocity of all distances. The gray triangle is considered as an outlier. With lower seepage velocities, the effective thermal retardation for the peak velocities starts to differ from the apparent retardation.

if R_{app} is applied. This is most likely due to the influence of thermal conduction on the thermal peak velocity. This has implications when heat is used as a tracer, for example in managed aquifer recharge systems, which could lead to an overestimation of the seepage velocity and therefore an underestimation of the mean transit time. Further research is required on the heat transfer between fluid and solid for natural material, e.g. influence of particle size mixtures etc., to clarify the effects of LTNE on the heat transport under these conditions. This could be done by using a thermal non-equilibrium model which would allow a more detailed investigation.

Declaration of Competing Interest

The authors declare that they have no known competing financial interests or personal relationships that could have appeared to influence the work reported in this paper.

Acknowledgments

This research was conducted within the GeoPot-project, which is financed by the Bavarian State Ministry of the Environment and Consumer Protection. We thank the two anonymous reviewers for their assessment which helped to improve the quality of this manuscript.

Appendix A. Supplementary data

Supplementary data to this article can be found online at https://doi.org/10.1016/j.jhydrol.2019.124097.

References

Adams, M.C., Davis, J., 1991. Kinetics of fluorescein decay and its application as a geothermal tracer. Geothermics 20, 53–66. https://doi.org/10.1016/0375-6505(91)90005-G.

Afshari, S., Hossein Hejazi, S., Kantzas, A., 2019. Pore-level modeling of effective longitudinal thermal dispersion in non-isothermal flows through granular porous media. Chem. Eng. Sci. 199, 451–462. https://doi.org/10.1016/j.ces.2019.01.028.

Anderson, M.P., 2005. Heat as a ground water tracer. Ground Water 43, 951–968. https://doi.org/10.1111/j.1745-6584.2005.00052.x.

Bakker, M., Caljé, R., Schaars, F., van der Made, K.-J., de Haas, S., 2015. An active heat tracer experiment to determine groundwater velocities using fiber optic cables installed with direct push equipment. Water Resour. Res. 51, 2760–2772. https://doi.org/10.1002/2014WR016632.

Bandai, T., Hamamoto, S., Rau, G.C., Komatsu, T., Nishimura, T., 2017. The effect of particle size on thermal and solute dispersion in saturated porous media. Int. J. Therm. Sci. 122, 1–38. https://doi.org/10.1016/j.ijthermalsci.2017.08.003.

Banks, D., 2015. A review of the importance of regional groundwater advection for ground heat exchange. Environ. Earth Sci. 73, 2555–2565. https://doi.org/10.1007/s12665-014-3377-4.

Barry, D.A., 2009. Effect of nonuniform boundary conditions on steady flow in saturated homogeneous cylindrical soil columns. Adv. Water Resour. 32, 522–531. https://doi.org/10.1016/j.advwatres.2009.01.003.

Bear, J., 1972. Dynamics of fluids in porous media. Soil Science. https://doi.org/10.1097/00010694-197508000-00022.

Becker, M.W., Bauer, B., Hutchinson, A., 2013. Measuring artificial recharge with fiber optic distributed temperature sensing. Groundwater 51, 670–678. https://doi.org/10.1111/j.1745-6584.2012.01006.x.

Becker, T.E., Clark, J.F., Johnson, T.A., 2015. Heat, B-10-enriched boric acid, and bromide as recycled groundwater tracers for managed aquifer recharge: case study. J. Hydrol. Eng. 20. https://doi.org/10.1061/(ASCE)HE.1943-5584.0001070.

Bekele, E., Patterson, B., Toze, S., Furness, A., Higginson, S., Shackleton, M., 2014. Aquifer residence times for recycled water estimated using chemical tracers and the propagation of temperature signals at a managed aquifer recharge site in Australia. Hydrogeol. J. 22, 1383–1401. https://doi.org/10.1007/s10040-014-1142-0.

Bodvarsson, G., 1972. Thermal problems in the siting of reinjection wells. Geothermics 1, 63–66. https://doi.org/10.1016/0375-6505(72)90013-2.

Bonner, R., Aylward, L., Harley, C., Kappelmeyer, U., Sheridan, C.M., 2017. Heat as a hydraulic tracer for horizontal subsurface flow constructed wetlands. J. Water Process Eng. 16, 183–192. https://doi.org/10.1016/j.jwpe.2017.01.007.

Böttcher, F., Casasso, A., Götzl, G., Zosseder, K., 2019. TAP - Thermal aquifer Potential: a quantitative method to assess the spatial potential for the thermal use of groundwater. Renew. Energy 142. https://doi.org/10.1016/j.renene.2019.04.086.

Buntebarth, G., Schopper, J.R., 1998. Experimental and theoretical investigations on the influence of fluids, solids and interactions between them on thermal properties of porous rocks. Phys. Chem. Earth 23, 1141–1146. https://doi.org/10.1016/S0079-1946(98)00142-6.

Caissie, D., Luce, C.H., 2017. Quantifying streambed advection and conduction heat fluxes. Water Resour. Res. 1595–1624. https://doi.org/10.1002/2016WR019813.

Constantz, J., 2010. Heat as a tracer to determine streambed water exchanges. Water Resour. Res. 46, 1–20. https://doi.org/10.1029/2008WR006996.

Constantz, J., Cox, M.H., Su, G.W., 2003. Comparison of heat and bromide as ground water tracers near streams. Groundwater 41, 647–656. https://doi.org/10.1111/j.1745-6584.2003.tb02403.x.

De Marsily, G., 1986. Quantitative Hydrogeology. Paris School of Mines, Fontainebleau.

Epting, J., García-Gil, A., Huggenberger, P., Vázquez-Suñe, E., Mueller, M.H., 2017. Development of concepts for the management of thermal resources in urban areas – Assessment of transferability from the Basel (Switzerland) and Zaragoza (Spain) case studies. J. Hydrol. 548, 697–715. https://doi.org/10.1016/j.jhydrol.2017.03.057.

Halloran, L.J.S., Rau, G.C., Andersen, M.S., 2016a. Heat as a tracer to quantify processes and properties in the vadose zone: a review. Earth-Science Rev. 159, 358–373. https://doi.org/10.1016/j.earscirev.2016.06.009.

Halloran, L.J.S., Roshan, H., Rau, G.C., Andersen, M.S., Acworth, R.I., 2016b. Improved spatial delineation of streambed properties and water fluxes using distributed temperature sensing. Hydrol. Process. 2702, 2686–2702. https://doi.org/10.1002/hyp.10806.

He, Y., 2005. Rapid thermal conductivity measurement with a hot disk sensor: Part 1. Theoretical considerations. Thermochim. Acta 436, 122–129. https://doi.org/10.1016/j.tca.2005.06.026.

Hermans, T., Nguyen, F., Klepikova, M., Dassargues, A., Caers, J., 2018. Uncertainty quantification of medium-term heat storage from short-term geophysical experiments using bayesian evidential learning. Water Resour. Res. 54, 2931–2948. https://doi.org/10.1002/2017WR022135.

Hoehn, E., Cirpka, O.A., 2006. Assessing hyporheic zone dynamics in two alluvial flood plains of the Southern Alps using water temperature and tracers. Hydrol. Earth Syst. Sci. 10, 553–563. https://doi.org/10.5194/hessd-3-335-2006.
Hopmans, J.W., Šimunek, J., Bristow, K.L., 2002. Indirect estimation of soil thermal properties and water flux using heat pulse probe measurements: Geometry and dispersion effects. Water Resour. Res. 38, 7–14. https://doi.org/10.1029/2000wr000071.
Irvine, D.J., Briggs, M.A., Lautz, L.K., Gordon, R.P., McKenzie, J.M., Cartwright, I., 2016. Using diurnal temperature signals to infer vertical groundwater-surface water exchange. Groundwater 55, 10–26. https://doi.org/10.1111/gwat.12459.
Irvine, D.J., Kurylyk, B.L., Cartwright, I., Bonham, M., Post, V.E.A., Banks, E.W., Simmons, C.T., 2017. Groundwater flow estimation using temperature-depth profiles in a complex environment and a changing climate. Sci. Total Environ. 574, 272–281. https://doi.org/10.1016/j.scitotenv.2016.08.212.
Irvine, D.J., Lautz, L.K., Briggs, M.A., Gordon, R.P., McKenzie, J.M., 2015. Experimental evaluation of the applicability of phase, amplitude, and combined methods to determine water flux and thermal diffusivity from temperature time series using VFLUX 2. J. Hydrol. 531, 728–737. https://doi.org/10.1016/j.jhydrol.2015.10.054.
Irvine, D.J., Simmons, C.T., Werner, A.D., Graf, T., 2013. Heat and solute tracers: how do they compare in heterogeneous aquifers? Groundwater 53, 10–20. https://doi.org/10.1111/gwat.12146.
Klepikova, M.V., Le Borgne, T., Bour, O., Dentz, M., Hochreutener, R., Lavenant, N., 2016a. Heat as a tracer for understanding transport processes in fractured media: theory and field assessment from multiscale thermal push-pull tracer tests. Water Resour. Res. 52, 5442–5457. https://doi.org/10.1002/2016WR018789.
Klepikova, M.V., Wildemeersch, S., Hermans, T., Jamin, P., Orban, P., Nguyen, F., Brouyère, S., Dassargues, A., 2016b. Heat tracer test in an alluvial aquifer: field experiment and inverse modelling. J. Hydrol. 540, 812–823. https://doi.org/10.1016/j.jhydrol.2016.06.066.
Klotz, D., Maloszewski, P., Moser, H., 1988. Mathematical modeling of radioactive tracer migration in water flowing through saturated porous media. Radiochim. Acta 44 (45), 373–379. https://doi.org/10.1524/ract.1988.4445.2.373.
Kurylyk, B.L., Irvine, D.J., Bense, V.F., 2018. Theory, tools, and multidisciplinary applications for tracing groundwater fluxes from temperature profiles. Wiley Interdiscip. Rev. Water 6. https://doi.org/10.1002/wat2.1329.
Laws, B.V., Dickenson, E.R.V., Johnson, T.A., Snyder, S.A., Drewes, J.E., 2011. Attenuation of contaminants of emerging concern during surface-spreading aquifer recharge. Sci. Total Environ. 409, 1087–1094. https://doi.org/10.1016/j.scitotenv.2010.11.021.
Leibundgut, C., Maloszewski, P., Külls, C., 2009. Tracers in Hydrology, Office. Wiley-Blackwell, West Sussex.
Lenda, A., Zuber, A., 1970. Tracer dispersion in groundwater experiments. Isot. Hydrol. 129, 619–636.
Levec, J., Carbonell, R.G., 1985. Longitudinal and lateral thermal dispersion in packed beds. Part II: comparison between theory and experiment. AIChE J. 31, 591–602. https://doi.org/10.1002/aic.690310408.
Lewandowski, J., Angermann, L., Nützmann, G., Fleckenstein, J.H., 2011. A heat pulse technique for the determination of small-scale flow directions and flow velocities in the streambed of sand-bed streams. Hydrol. Process. 25, 3244–3255. https://doi.org/10.1002/hyp.8062.
Lo Russo, S., Taddia, G., 2010. Advective heat transport in an unconfined aquifer induced by the field injection of an open-loop groundwater heat pump. Am. J. Environ. Sci. 6, 253–259. https://doi.org/10.3844/ajessp.2010.253.259.
Ma, R., Zheng, C., 2010. Effects of density and viscosity in modeling heat as a groundwater tracer. Ground Water 48, 380–389. https://doi.org/10.1111/j.1745-6584.2009.00660.x.
Ma, R., Zheng, C., Zachara, J.M., Tonkin, M., 2012. Utility of bromide and heat tracers for aquifer characterization affected by highly transient flow conditions. Water Resour. Res. 48, 1–18. https://doi.org/10.1029/2011WR011281.
Markle, J.M., Schincariol, R.A., 2007. Thermal plume transport from sand and gravel pits – Potential thermal impacts on cool water streams. J. Hydrol. 338, 174–195. https://doi.org/10.1016/j.jhydrol.2007.02.031.
Maya, S.M., García-Gil, A., Schneider, E.G., Moreno, M.M., Epting, J., Vázquez-Suñé, E., Marazuela, M.Á., Sánchez-Navarro, J.Á., 2018. An upscaling procedure for the optimal implementation of open-loop geothermal energy systems into hydrogeological models. J. Hydrol. 563, 155–166. https://doi.org/10.1016/j.jhydrol.2018.05.057.
Metzger, T., Didierjean, S., Maillet, D., 2004. Optimal experimental estimation of thermal dispersion coefficients in porous media. Int. J. Heat Mass Transf. 47, 3341–3353. https://doi.org/10.1016/j.ijheatmasstransfer.2004.02.024.
Moeck, C., Radny, D., Popp, A., Brennwald, M., Stoll, S., Auckenthaler, A., Berg, M., Schirmer, M., 2017. Characterization of a managed aquifer recharge system using multiple tracers. Sci. Total Environ. 609, 701–714. https://doi.org/10.1016/j.scitotenv.2017.07.211.
Nagano, K., Mochida, T., Ochifuji, K., 2002. Influence of natural convection on forced horizontal flow in saturated porous media for aquifer thermal energy storage. Appl. Therm. Eng. 22, 1299–1311. https://doi.org/10.1016/S1359-4311(02)00056-X.
Pan, M., Huang, Q., Feng, R., Xu, X., Xiong, Y., Huang, G., 2019. Improving the estimation of hydraulic and thermal properties of heterogeneous media via the addition of heat loss. Vadose Zo. J. 18. https://doi.org/10.2136/vzj2018.08.0149.
Park, B.H., Bae, G.O., Lee, K.K., 2015. Importance of thermal dispersivity in designing groundwater heat pump (GWHP) system: Field and numerical study. Renew. Energy 83, 270–279. https://doi.org/10.1016/j.renene.2015.04.036.
Park, B.H., Lee, B.H., Lee, K.K., 2018. Experimental investigation of the thermal dispersion coefficient under forced groundwater flow for designing an optimal groundwater heat pump (GWHP) system. J. Hydrol. 562, 385–396. https://doi.org/10.1016/j.jhydrol.2018.05.023.
Rau, G.C., Andersen, M.S., Acworth, R.I., 2012a. Experimental investigation of the thermal dispersivity term and its significance in the heat transport equation for flow in sediments. Water Resour. Res. 48, 1–21. https://doi.org/10.1029/2011WR011038.
Rau, G.C., Andersen, M.S., Acworth, R.I., 2012b. Experimental investigation of the thermal time-series method for surface water-groundwater interactions. Water Resour. Res. 48, 1–18. https://doi.org/10.1029/2011WR011560.
Rau, G.C., Andersen, M.S., McCallum, A.M., Roshan, H., Acworth, R.I., 2014. Heat as a tracer to quantify water flow in near-surface sediments. Earth-Science Rev. 129, 40–58. https://doi.org/10.1016/j.earscirev.2013.10.015.
Rau, G.C., Halloran, L.J.S., Cuthbert, M.O., Andersen, M.S., Acworth, R.I., Tellam, J.H., 2017. Characterising the dynamics of surface water-groundwater interactions in intermittent and ephemeral streams using streambed thermal signatures. Adv. Water Resour. 107, 354–369. https://doi.org/10.1016/j.advwatres.2017.07.005.
Ren, J., Cheng, J., Yang, J., Zhou, Y., 2018. A review on using heat as a tool for studying groundwater–surface water interactions. Environ. Earth Sci. 77, 1–13. https://doi.org/10.1007/s12665-018-7959-4.
Roshan, H., Cuthbert, M.O., Andersen, M.S., Acworth, R.I., 2014. Local thermal non-equilibrium in sediments: implications for temperature dynamics and the use of heat as a tracer. Adv. Water Resour. 73, 176–184. https://doi.org/10.1016/j.advwatres.2014.08.002.
Runkel, R.L., 1996. Solution of the Advection-Dispersion Equation: Continous Load of Finite Duration. J. Environ. Engenieering 122, 830–832. https://doi.org/10.1061/(ASCE)0733-9372(1996) 122.
Saar, M.O., 2010. Review: geothermal heat as a tracer of large-scale groundwater flow and as a means to determine permeability fields. Hydrogeol. J. 19, 31–52. https://doi.org/10.1007/s10040-010-0657-2.
Sarris, T.S., Close, M., Abraham, P., 2018. Using solute and heat tracers for aquifer characterization in a strongly heterogeneous alluvial aquifer. J. Hydrol. 558, 55–71. https://doi.org/10.1016/j.jhydrol.2018.01.032.
Scharli, U., Rybach, L., 2001. Determination of specific heat capacity on rock fragments. Geothermics 30, 93–110. https://doi.org/10.1016/S0375-6505(00)00035-3.
Schincariol, R.A., Schwartz, F.W., 1990. An experimental investigation of variable density flow and mixing in homogeneous and heterogeneous media. Water Resour. Res. 26, 2317–2329. https://doi.org/10.1029/WR026i010p02317.
Schneidewind, U., van Berkel, M., Anibas, C., Vandersteen, G., Schmidt, C., Joris, I., Seuntjens, P., Batelaan, O., Zwart, H.J., 2016. LPMLE3: A novel 1-D approach to study water flow in streambeds using heat as a tracer. Water Resour. Res. 52, 5951–5970. https://doi.org/10.1002/2015WR018389.Received.
Seibert, S., Prommer, H., Siade, A., Harris, B., Trefry, M., Martin, M., 2014. Heat and mass transport during a groundwater replenishment trial in a highly heterogeneous aquifer. Water Resour. Res. 50, 9463–9483. https://doi.org/10.1002/2013WR015219.
Seibertz, K.S.O., Chirila, M.A., Bumberger, J., Dietrich, P., Vienken, T., 2016. Development of in-aquifer heat testing for high resolution subsurface thermal-storage capability characterisation. J. Hydrol. 534, 113–123. https://doi.org/10.1016/j.jhydrol.2015.12.013.
Shook, G.M., 2001. Predicting thermal breakthrough in heterogeneous media from tracer tests. Geothermics 30, 573–589. https://doi.org/10.1016/S0375-6505(01)00015-3.
Smart, P.L., Laidlaw, I.M.S., 1977. An evaluation of some fluorescent dyes for water tracing. Water Resour. Res. 13, 15–33. https://doi.org/10.1029/WR013i001p00015.
Somogyvári, M., Bayer, P., 2017. Field validation of thermal tracer tomography for reconstruction of aquifer heterogeneity. Water Resour. Res. 53, 5375–5377. https://doi.org/10.1002/2013WR014979.Reply.
Somogyvári, M., Bayer, P., Brauchler, R., 2016. Travel-time-based thermal tracer tomography. Hydrol. Earth Syst. Sci. 20, 1885–1901. https://doi.org/10.5194/hess-20-1885-2016.
Stauffer, F., Bayer, P., Blum, P., Molina-Giraldo, N., Kinzelbach, W., 2013. Thermal Use of Shallow Groundwater. CRC Press, Boca Raton.
Taniguchi, M., Sharma, M.L., 1990. Solute and heat transport experiments for estimating recharge rate. J. Hydrol. 119, 57–69. https://doi.org/10.1016/0022-1694(90)90034-U.
Tarnawski, V.R., Momose, T., Leong, W.H., 2011. Thermal conductivity of standard sands II. Saturated conditions. Int. J. Thermophys. 32, 984–1005. https://doi.org/10.1007/s10765-011-0975-1.
Taylor, K., Banks, D., Watson, I., 2016. Heat as a natural, low-cost tracer in mine water systems: The attenuation and retardation of thermal signals in a Reducing and Alkalinity Producing Treatment System (RAPS). J. Coal Geol. Int. https://doi.org/10.1016/j.coal.2016.03.013.
Toride, N., Leij, F.J., van Genuchten, M.T., 1995. The CXTFIT Code for Estimating Transport Parameters from Laboratory or Field Tracer Experiments.
van Genuchten, M.T., Alves, W.J., 1982. Analytical solutions of the one-dimensional convective-dispersive solute transport equation. Agric. Res. Serv. Tech. Bull. 1661.
Vandenbohede, A., Louwyck, A., Lebbe, L., 2009. Conservative solute versus heat transport in porous media during push-pull tests. Transp. Porous Media 76, 265–287. https://doi.org/10.1007/s11242-008-9246-4.
Vandenbohede, A., Van Houtte, E., 2012. Heat transport and temperature distribution during managed artificial recharge with surface ponds. J. Hydrol. 472–473, 77–89.

https://doi.org/10.1016/j.jhydrol.2012.09.028.
VDI, 2013. VDI-Wärmeatlas. doi:10.1007/978-3-642-19981-3.
Visser, P.W., Kooi, H., Stuyfzand, P.J., 2015. The thermal impact of aquifer thermal energy storage (ATES) systems: a case study in the Netherlands, combining monitoring and modeling. Hydrogeol. J. 23, 507–532. https://doi.org/10.1007/s10040-014-1224-z.
Wagner, V., Li, T., Bayer, P., Leven, C., Dietrich, P., Blum, P., 2013. Thermal tracer testing in a sedimentary aquifer: field experiment (Lauswiesen, Germany) and numerical simulation. Hydrogeol. J. 22, 175–187. https://doi.org/10.1007/s10040-013-1059-z.
Wildemeersch, S., Jamin, P., Orban, P., Hermans, T., Klepikova, M.V., Nguyen, F., Brouyère, S., Dassargues, A., 2014. Coupling heat and chemical tracer experiments for estimating heat transfer parameters in shallow alluvial aquifers. J. Contam. Hydrol. 169, 90–99. https://doi.org/10.1016/j.jconhyd.2014.08.001.
Woods, A.W., Fitzgerald, S.D., 1997. The vaporization of a liquid front moving through a hot porous rock. Part 2 Slow injection. J. Fluid Mech. 3443, 303–316. https://doi.org/10.1017/S0022112093003520.
Woods, A.W., Fitzgerald, S.D., 1993. The vaporization of a liquid front moving through a hot porous rock. J. Fluid Mech. 251, 563–579. https://doi.org/10.1017/S0022112093003520.
Zhang, X., Liu, W., Liu, Z., 2009. Criterion for Local Thermal Equilibrium in Forced Convection Flow Through Porous Media. J. Porous Media 12, 1103–1111. https://doi.org/10.1615/JPorMedia.v12.i11.60.